International Journal of Engineering Science 47 (2009) 141–152

Contents lists available at ScienceDirect

International Journal of Engineering Science

journal homepage: www.elsevier.com/locate/ijengsci

Annular axisymmetric stagnation flow on a moving cylinder

Liu Hong [a], C.Y. Wang [b,*]

[a] Zhou Pei-Yuan Center for Applied Mathematics, Tsinghua University, Beijing, China
[b] Departments of Mathematics and Mechanical Engineering, Michigan State University, Abbott Road, East Lansing, MI 48824, USA

ARTICLE INFO

Article history:
Received 23 January 2008
Received in revised form 11 August 2008
Accepted 13 August 2008
Available online 25 September 2008

Communicated by K.R. Rajagopal

Keywords:
Stagnation flow
Cylinder
Similarity

ABSTRACT

Fluid is injected from a fixed outer cylindrical casing onto an inner moving cylindrical rod. Using similarity transform, the Navier–Stokes equations reduce to a set of nonlinear ordinary differential equations, which are integrated numerically. Asymptotic solutions for large and small cross-flow Reynolds numbers and small gap widths are also found. Drag, torque and heat transfer on the moving rod are determined. The problem is particularly important in pressure-lubricated bearings.

1. Introduction

Similarity solutions of the Navier–Stokes equations are rare [1]. The basic similarity solution describing two-dimensional stagnation flow towards a plate was introduced by Hiemenz [2]. The similarity solution for the axisymmetric stagnation flow on a circular cylinder was found by Wang [3]. Gorla [4] extended the solution to include axial translation of the cylinder while Cunning et al. [5] studied the axial rotation and transpiration on the cylinder. The previous literature considered a stagnation flow originated from infinity. In the present paper, the stagnation flow in the annular region between two cylinders is studied. Fluid is injected inward radially from a fixed outer cylinder towards an axially translating and rotating inner cylinder. Such finite geometry is more realistic for the convective cooling of a moving rod [6]. The problem also models externally pressure-lubricated journal bearings which are quite attractive for high speed and miniature rotating systems [7–11]. The aim of the present paper is to find a similarity stagnation flow for the annular region.

2. Formulation

Fig. 1 shows a vertical inner cylinder (shaft) of radius R rotating with angular velocity Ω and moving with velocity W in the axial z-direction. The inner cylinder is enclosed by an outer cylinder (bushing) of radius bR. Fluid is injected radially with velocity U from the outer cylinder towards the inner cylinder. Assuming end effects can be ignored (long cylinders), the flow is axisymmetric about the z-axis.

The constant property continuity equation and the constant property Navier–Stokes equations in axisymmetric cylindrical coordinates are:

* Corresponding author.
E-mail address: cywang@mth.msu.edu (C.Y. Wang).

0020-7225/$ - see front matter © 2008 Elsevier Ltd. All rights reserved.
doi:10.1016/j.ijengsci.2008.08.002

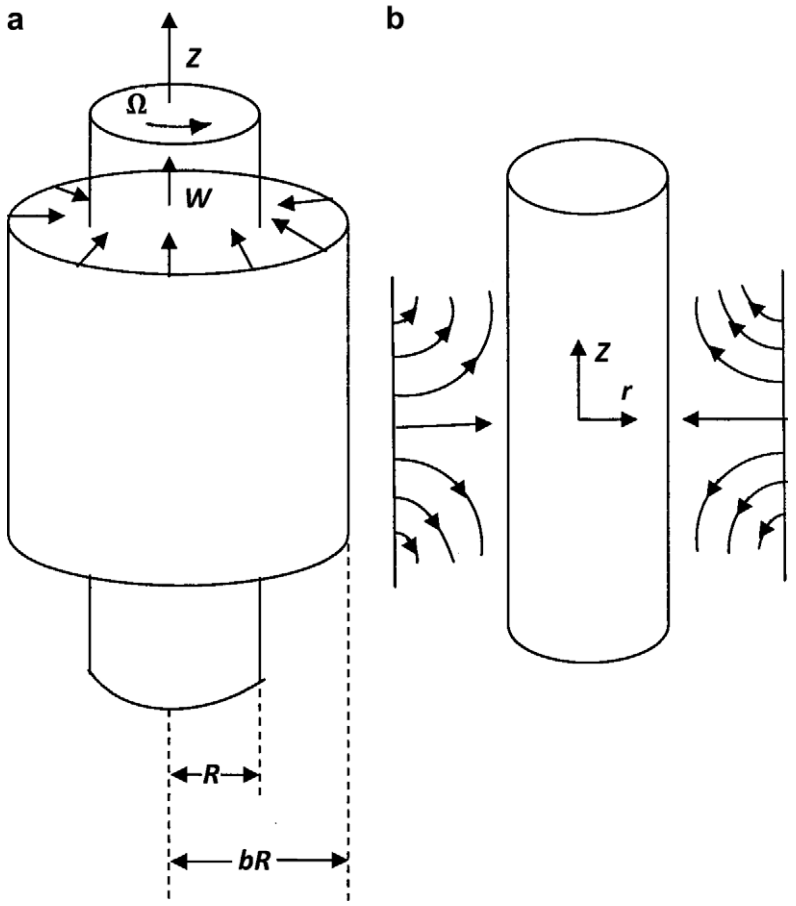

Fig. 1. Annular axisymmetric stagnation flow on a moving cylinder. (a) The inner cylinder rotates with angular velocity Ω and move axially with velocity W. The outer cylinder is fixed with fluid injected towards the inner cylinder. (b) Cross section showing streamlines in the annular region.

$$rw_z + (ru)_r = 0 \tag{1}$$

$$uu_r + wu_z - \frac{v^2}{r} = -\frac{p_r}{\rho} + \nu\left(u_{rr} + \frac{u_r}{r} + u_{zz} - \frac{u}{r^2}\right) \tag{2}$$

$$uv_r + wv_z + \frac{uv}{r} = \nu\left(v_{rr} + \frac{v_r}{r} + v_{zz} - \frac{v}{r^2}\right) \tag{3}$$

$$uw_r + ww_z = -\frac{p_z}{\rho} + \nu\left(w_{rr} + \frac{w_r}{r} + w_{zz}\right) \tag{4}$$

Here (u, v, w) are velocity components in the cylindrical coordinates (r, θ, z) directions, respectively, ν is the kinematic viscosity, ρ is the density and p is the pressure.

Extending the work of Wang [3], the following similarity transform is suggested

$$u = -Uf(\eta)/\sqrt{\eta}, \quad v = \Omega a h(\eta), \quad w = 2Uf'(\eta)\xi + Wg(\eta) \tag{5}$$

$$\eta = \frac{r^2}{R^2}, \quad \xi = \frac{z}{R} \tag{6}$$

Eq. (1) is automatically satisfied. Eliminating pressure, Eqs. (2)–(4) become

$$\eta f'''' + 2f''' + Re(ff''' - f'f'') = 0 \tag{7}$$

$$\eta g'' + g' + Re(fg' - f'g) = 0 \tag{8}$$

$$4\eta h'' + 4h' - \frac{h}{\eta} + Re\left(4fh' + \frac{2fh}{\eta}\right) = 0 \tag{9}$$

Here $Re = Ua/2v$ is the cross-flow Reynolds number. The pressure can be recovered by

$$p = p_s - \rho\left[\frac{U^2 f^2}{2\eta} + \frac{U^2 f'}{Re} - \frac{\Omega^2 R^2}{2}\int_1^\eta \frac{h^2(\tau)}{\tau}\mathrm{d}\tau + 2C_0 U^2 \xi^2\right] \tag{10}$$

where p_s is the stagnation pressure, and $C_0 = f''(1) + f''(1)$. The boundary conditions are no slip on the inner cylinder

$$f(1) = 0, \quad f'(1) = 0 \tag{11}$$
$$g(1) = 1, \quad h(1) = 1 \tag{12}$$

and uniform injection on the outer cylinder

$$f(b) = \sqrt{b}, \quad f'(b) = 0 \tag{13}$$
$$g(b) = 0, \quad h(b) = 0 \tag{14}$$

Although Eqs. (7), (11) and (13) are decoupled from the other equations, the system is still formidable. In what follows we shall develop some approximate solutions before integrating the similarity equations Eqs. (7)–(9) and (11)–(14) numerically.

3. Asymptotic solution for small Reynolds numbers

This is the case when the injection velocity is small, or the diameter of the inner cylinder is small, or the viscosity is large. We expand in terms of Reynolds number $Re \ll 1$.

$$f = f_0 + Ref_1 + \cdots \tag{15}$$
$$g = g_0 + Reg_1 + \cdots, \quad h = h_0 + Reh_1 + \cdots \tag{16}$$

Eqs. (7)–(9) lead to the zeroth order equations

$$\eta f_0'''' + 2f_0'' = 0 \tag{17}$$
$$\eta g_0'' + g_0' = 0 \tag{18}$$
$$4\eta h_0'' + 4h_0' - \frac{h_0}{\eta} = 0 \tag{19}$$

with the boundary conditions

$$f_0(1) = f_0'(1) = f_0'(b) = 0, \quad f_0(b) = \sqrt{b} \tag{20}$$
$$g_0(1) = 1, \quad g_0(b) = 0 \tag{21}$$
$$h_0(1) = 1, \quad h_0(b) = 0 \tag{22}$$

The solutions are

$$f_0 = \frac{\sqrt{b}[-2(b-1)\eta\ln\eta + \ln b\cdot\eta^2 + 2(b-1-\ln b)\eta - (2b-2-\ln b)]}{(b-1)[2(b-1)-(b+1)\ln b]} \tag{23}$$
$$g_0 = -\frac{\ln\eta}{\ln b} + 1 \tag{24}$$
$$h_0 = \frac{\eta - b}{(1-b)\sqrt{\eta}} \tag{25}$$

The first order equations are

$$\eta f_1'''' + 2f_1'' = f_0' f_0'' - f_0 f_0''' \tag{26}$$
$$\eta g_1'' + g_1' = f_0' g_0 - f_0 g_0' \tag{27}$$
$$4\eta h_1'' + 4h_1' - \frac{h_1}{\eta} = -4f_0 h_0' - \frac{2f_0 h_0}{\eta} \tag{28}$$

with zero boundary conditions. The solutions are complicated but straight forward, and will not be presented here (see Appendix). However, they are used in the comparison with the exact numerical solution in a later section. Fig. 2 shows some typical profiles of the first order functions. The Appendix gives the analytic forms obtained by a computer with symbolic capability.

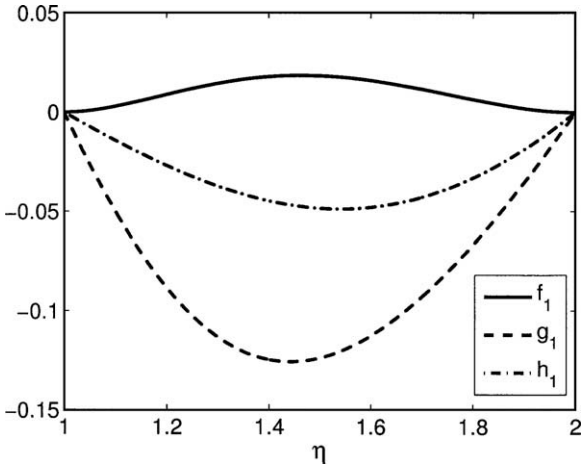

Fig. 2. Inertial corrections f_1, g_1, h_1 defined in Eqs. (15) and (16) and the Appendix ($b = 2$).

Thus we find analytically

$$f''(1) = \frac{2\sqrt{b}[\ln b - (b+1)]}{(b-1)[2(b-1) - (b+1)\ln b]} + Ref_1''(1) + O(Re^2) \tag{29}$$

$$f'''(1) = \frac{2\sqrt{b}}{2(b-1) - (b+1)\ln b} + Ref_1'''(1) + O(Re^2) \tag{30}$$

$$g'(1) = -\frac{1}{\ln b} + Reg_1'(1) + O(Re^2) \tag{31}$$

$$h'(1) = -\frac{b+1}{2(b-1)} + Reh_1'(1) + O(Re^2) \tag{32}$$

4. Asymptotic solution for large Reynolds numbers

If $Re \gg 1$, the radial inertial effects are much more important than the viscous effect. We expect the radial injection is almost potential except in a boundary layer of order $(Re^{-1/2})$ near the inner cylinder where the tangential velocity is brought to zero.

Consider the normal flow first. For the outer flow we expand directly

$$f = F + O(Re^{-1/2}) \tag{33}$$

Eq. (7) becomes

$$FF''' - F'F'' = 0 \tag{34}$$

The boundary conditions are

$$F(1) = 0, \quad F(b) = \sqrt{b}, \quad F'(b) = 0 \tag{35}$$

where we have relaxed the tangential boundary conditions on the inner cylinder.

The solution to Eqs. (34) and (35) is

$$F = \sqrt{b}\cos\left[\left(\frac{b-\eta}{b-1}\right)\left(n - \frac{1}{2}\right)\pi\right] \tag{36}$$

giving

$$F'(1) = (-1)^{n+1}\lambda, \quad \lambda = \left(\frac{\sqrt{b}}{b-1}\right)\left(n - \frac{1}{2}\right)\pi \tag{37}$$

The integer n is taken to be unity since we do not expect flow reversals in the annulus.

In the boundary layer, set

$$f = \sqrt{\frac{\lambda}{Re}}\varphi(\varsigma) + O(Re^{-1}), \quad \varsigma = \sqrt{\lambda Re}(\eta - 1) \tag{38}$$

Then Eqs. (7), (11) and (13) yield the Hiemenz boundary layer equation

$$\varphi''' + \varphi\varphi'' - \varphi'^2 + 1 = 0 \tag{39}$$

$$\varphi(0) = \varphi'(0) = 0, \quad \varphi'(\infty) = 1 \tag{40}$$

The solution to Eqs. (39) and (40) is well known (e.g. [12]). We find

$$\varphi''(0) = 1.232588, \quad \varphi(\infty) \sim \varsigma - 0.6479 \tag{41}$$

A uniformly valid solution is then constructed

$$f = \sqrt{b}\cos\left[\left(\frac{b-\eta}{b-1}\right)\frac{\pi}{2}\right] + \sqrt{\frac{\lambda}{Re}}[\varphi(\varsigma) - \varsigma] + \cdots \tag{42}$$

From which we find the boundary derivatives

$$f''(1) = \lambda\sqrt{\lambda Re}\varphi''(0) = 1.232588\lambda\sqrt{\lambda Re} \tag{43}$$

$$f'''(1) = -\lambda^2 Re - \frac{\lambda^3}{b} + \cdots \tag{44}$$

Similarly, let

$$g = G + O(Re^{-1/2}), \quad h = H + O(Re^{-1/2}) \tag{45}$$

The outer flow yields

$$G = 0, \quad H = 0 \tag{46}$$

In the boundary layer, let

$$g = \psi(\varsigma), \quad h = \theta(\varsigma) \tag{47}$$

And from Eqs. (8) and (9) we obtain the boundary layer equations

$$\psi'' + \varphi\psi' - \varphi'\psi = 0 \tag{48}$$

$$\theta'' + \varphi\theta' = 0 \tag{49}$$

The boundary conditions are

$$\psi(0) = 1, \quad \psi(\infty) = 0 \tag{50}$$

$$\theta(0) = 1, \quad \theta(\infty) = 0 \tag{51}$$

Since the function for φ is known, Eqs. (48)–(51) are integrated numerically, resulting in universal (no parameter dependence) solutions for ψ and θ. We find $\psi'(0) = -0.81130$ and $\theta'(0) = -0.57045$. Thus the analytic boundary derivatives are

$$g'(1) = -0.81130\sqrt{\lambda Re} + \cdots \tag{52}$$

$$h'(1) = -0.57045\sqrt{\lambda Re} + \cdots \tag{53}$$

The universal curves of φ, ψ, and θ are shown in Fig. 3.

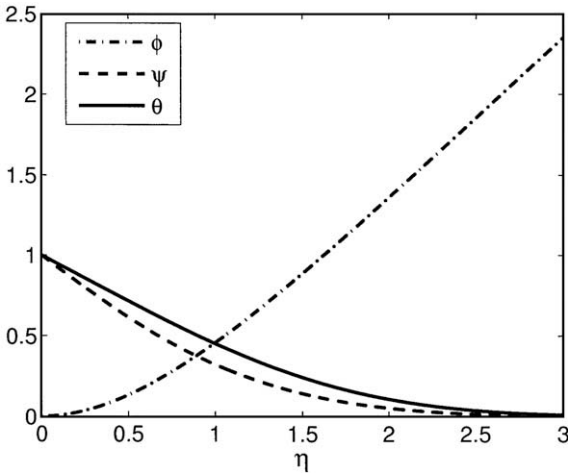

Fig. 3. The universal curves of φ, ψ, and θ. φ is the Hiemenz solution, ψ and θ are functions due to the motion of the inner cylinder. See Eqs. (5) and (47).

5. Perturbation solution for small gap width

This case models bearings with fluid injection. When the annulus gap width is small, set $\varepsilon = b - 1 \ll 1$ and

$$\eta = 1 + \varepsilon\sigma, \quad 0 \leqslant \sigma \leqslant 1 \tag{54}$$

Expand

$$f = \Phi_0(\sigma) + \varepsilon\Phi_1(\sigma) + \cdots, \quad g = \Psi_0(\sigma) + \varepsilon\Psi_1(\sigma) + \cdots, \quad h = \Lambda_0(\sigma) + \varepsilon\Lambda_1(\sigma) + \cdots \tag{55}$$

We assume the cross-flow Reynolds number is not too large. Eqs. (7)–(9) and (11)–(14) yield the zeroth order

$$\Phi_0'''' = 0, \quad \Psi_0'' = 0, \quad \Lambda_0'' = 0 \tag{56}$$

with the boundary conditions

$$\Phi_0(0) = 1, \quad \Phi_0'(0) = 0, \quad \Phi_0(1) = 1, \quad \Phi_0'(1) = 0 \tag{57}$$

$$\Psi_0(0) = 1, \quad \Psi_0(1) = 0, \quad \Lambda_0(0) = 1, \quad \Lambda_0(1) = 0 \tag{58}$$

The solutions are

$$\Phi_0 = 3\sigma^2 - 2\sigma^3, \quad \Psi_0 = 1 - \sigma, \quad \Lambda_0 = 1 - \sigma \tag{59}$$

The first order equations are

$$\Phi_1'''' = -2\Phi_0''' - Re(\Phi_0\Phi_0''' - \Phi_0'\Phi_0'') \tag{60}$$

$$\Psi_1'' = -\Psi_0' - Re(\Phi_0\Psi_0' - \Phi_0'\Psi_0) \tag{61}$$

$$\Lambda_1'' = -\Lambda_0' - Re\Phi_0\Lambda_0' \tag{62}$$

With the boundary conditions

$$\Phi_1(0) = 0, \quad \Phi_1'(0) = 0, \quad \Phi_1(1) = 1/2, \quad \Phi_1'(1) = 0 \tag{63}$$

$$\Psi_1(0) = 0, \quad \Psi_1(1) = 0, \quad \Lambda_1(0) = 0, \quad \Lambda_1(1) = 0 \tag{64}$$

The solutions are

$$\Phi_1 = \frac{5}{2}\sigma^2 - 3\sigma^3 + \sigma^4 + Re\left(\frac{8}{35}\sigma^2 - \frac{27}{70}\sigma^3 + \frac{3}{10}\sigma^5 - \frac{1}{5}\sigma^6 + \frac{2}{35}\sigma^7\right) \tag{65}$$

$$\Psi_1 = -\frac{1}{2}\sigma + \frac{1}{2}\sigma^2 + Re\left(-\frac{9}{20}\sigma + \sigma^3 + \frac{3}{10}\sigma^5 - \frac{3}{4}\sigma^4 + \frac{1}{5}\sigma^5\right) \tag{66}$$

$$\Lambda_1 = -\frac{1}{2}\sigma + \frac{1}{2}\sigma^2 + Re\left(-\frac{3}{20}\sigma + \frac{1}{4}\sigma^4 - \frac{1}{10}\sigma^5\right) \tag{67}$$

The approximate boundary derivatives are then

$$f''(1) = \frac{1}{\varepsilon^2}\left[\Phi_0''(0) + \varepsilon\Phi_1''(0) + \cdots\right] = \frac{1}{\varepsilon^2}\left[6 + \varepsilon\left(5 + \frac{16}{35}Re\right) + \cdots\right] \tag{68}$$

$$f'''(1) = \frac{1}{\varepsilon^3}\left[\Phi_0'''(0) + \varepsilon\Phi_1'''(0) + \cdots\right] = \frac{1}{\varepsilon^3}\left[-12 - \varepsilon\left(18 + \frac{81}{35}Re\right) + \cdots\right] \tag{69}$$

$$g'(1) = \frac{1}{\varepsilon}\left[\Psi_0''(0) + \varepsilon\Psi_1''(0) + \cdots\right] = \frac{1}{\varepsilon}\left[-1 - \varepsilon\left(\frac{1}{2} + \frac{9}{20}Re\right) + \cdots\right] \tag{70}$$

$$h'(1) = \frac{1}{\varepsilon}\left[\Lambda_0''(0) + \varepsilon\Lambda_1''(0) + \cdots\right] = \frac{1}{\varepsilon}\left[-1 - \varepsilon\left(\frac{1}{2} + \frac{3}{20}Re\right) + \cdots\right] \tag{71}$$

6. Numerical solution and comparison of results

The exact numerical integration of the similarity equations is described as follows. Given the cross-flow Reynolds number Re and the gap width $b - 1 > 0$, together with a guessed boundary derivatives for $f''(1)$ and $f'''(1)$, Eq. (7) is integrated as an initial value problem by a standard Runge–Kutta algorithm. The boundary derivatives are guided by our analytic approximate solutions. When $\eta = b$ we check whether Eq. (13) is satisfied. Through two-dimensional shooting with Newton's correction, one can obtain the boundary derivatives fairly accurately. The relative error is kept under 10^{-6}. Then using the solution for f, we integrate either Eq. (8) or Eq. (9) for the functions g or h. The initial conditions are Eq. (12) with a guessed $g'(1)$ or $h'(1)$. The solution is found when Eq. (14) is satisfied. Some representative curves for the functions f, g, h are given in Figs. 4–6. Our numerical solution of the ordinary differential equations, similar to Hiemenz's [2] work, constitutes an exact similarity solution of the Navier–Stokes equations.

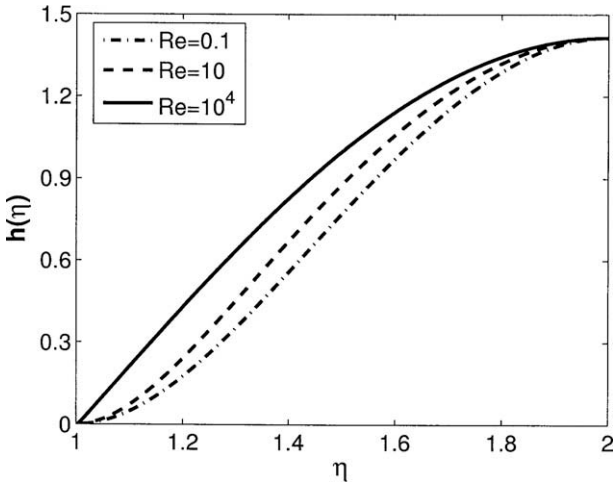

Fig. 4. Similarity function $f(\eta)$ under different Reynolds numbers, numerically integrated with $b = 2$.

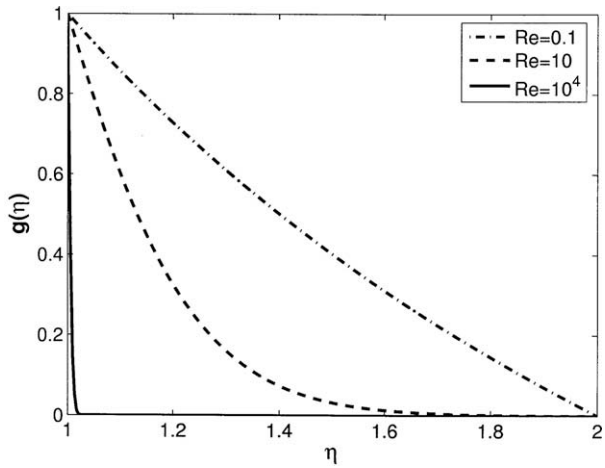

Fig. 5. Similarity function $g(\eta)$ under different Reynolds numbers, numerically integrated with $b = 2$.

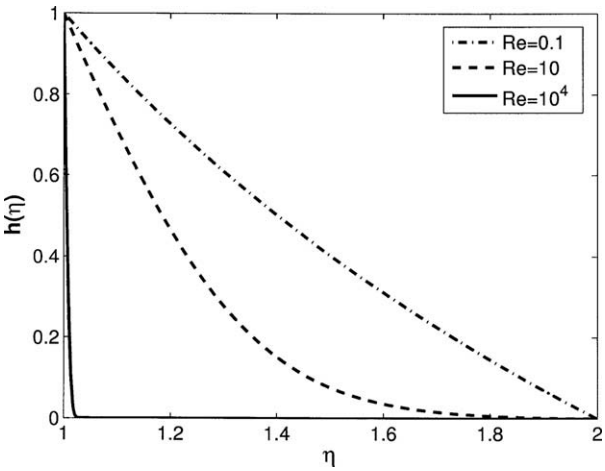

Fig. 6. Similarity function $h(\eta)$ under different Reynolds numbers, numerically integrated with $b = 2$.

Table 1
The boundary derivatives $f'(1)$, $f''(1)$, $g'(1)$, $h'(1)$

$f'(1)$	$b = 1.1$				$b = 2$				$b = 10$			
Re	Numer	Small *Re*	Large *Re*	Small gap	Numer	Small *Re*	Large *Re*	Small gap	Numer	Small *Re*	Large *Re*	Small gap
0.1	650.3526	650.352		650.457	11.0010	11.001		11.0457	0.667	0.6674		0.634
1	654.7679	654.770		654.571	11.6772	11.684		11.4571	0.863	0.8938		0.680
10	698.6176	698.951		695.714	17.5348	18.519		15.5714	1.867		1.598	
100	1082.300	1140.800	824.218	1107.100	44.4492		40.810		5.292		5.054	
1000	2819.700		2606.400		132.436		129.053		16.210		15.982	
10000	8447.300		8242.200		411.373		408.103		50.764		50.539	
$f''(1)$	$b = 1.1$				$b = 2$				$b = 10$			
Re	Numer	Small *Re*	Large *Re*	Small gap	Numer	Small *Re*	Large *Re*	Small gap	Numer	Small *Re*	Large *Re*	Small gap
0.1	−13883	−13883		−13823	−36.1443	−36.143		−30.2314	−0.9172	−0.917		−0.241
1	−14117	−14116		−14031	−41.0797	−41.000		−32.3143	−1.3924	−1.405		−0.267
10	−16507	−16452		−16114	−93.5670	−89.565			−5.2400	−6.287		
100	−42933	−39806		−36943	−590.738	−575.21			−36.4750		−30.478	
1000	−305970	−273350	−275480	−245230	−5211.80	−5431.7	−4940.30		−322.795		−304.63	
10000	−2813200		−2718200		−50187.0		−49354.0		−3102.90		−3046.2	
$g'(1)$	$b = 1.1$				$b = 2$				$b = 10$			
Re	Numer	Small *Re*	Large *Re*	Small gap	Numer	Small *Re*	Large *Re*	Small gap	Numer	Small *Re*	Large *Re*	Small gap
0.1	−10.5382	−10.538		−10.545	−1.4963	−1.496		−1.545	−0.5080	−0.514		−0.656
1	−10.9489	−10.948		−10.950	−1.9309	−1.984		−1.950	−0.9040	−1.234		−1.061
10	−14.6586	−14.658		−15.000	−4.3856		−3.823	−6.000	−2.2168		−1.906	
100	−35.7103	−35.710	−32.929		−12.6450		−12.092		−6.3381		−6.027	
1000	−106.9611	−106.961	−104.133		−38.7853		−38.238		−19.3699		−19.059	
10000	−332.1775		−329.299		−121.452		−120.920		−60.5821		−60.272	
$h'(1)$	$b = 1.1$				$b = 2$				$b = 10$			
Re	Numer	Small *Re*	Large *Re*	Small gap	Numer	Small *Re*	Large *Re*	Small gap	Numer	Small *Re*	Large *Re*	Small gap
0.1	−10.5151	−10.515		−10.515	−1.5151	−1.515		−1.515	−0.6235	−0.623		−0.626
1	−10.6511	−10.650		−10.650	−1.6554	−1.650		−1.650	−0.7570	−0.731		−0.761
10	−12.0407	−12.007		−12.000	−3.0517	−3.007	−2.7056	−3.000	−1.5941	−1.809	−1.348	
100	−24.8226	−25.570	−23.300	−25.500	−8.8636		−8.5559		−4.4487		−4.264	
1000	−75.1076		−73.681		−27.2421		−27.0562		−13.5959		−13.486	
10000	−233.5209		−231.540		−85.3916		−85.0227		−42.5694		−42.379	

Values from exact numerical integration are compared with those from small Reynolds number approximation, large Reynolds number approximation and small gap approximation.

Table 1 shows a comparison of the exact numerical initial values thus obtained and the initial values using our analytic approximate values. We see that the small Reynolds number approximation, Eqs. (29)–(32) is satisfactory for $Re < 1$, and the range may be extended to larger *Re* in certain cases. The large Reynolds number approximation, Eqs. (43), (44), (52) and (53) are good mostly for $Re \geqslant 1000$. On the other hand, the small gap width approximation, Eqs. (68)–(71) compares well if $b < 2$ and moderate Reynolds numbers (we assumed $Re = O(1)$ in the expansions).

From Eq. (1) a stream function χ can be defined

$$u = -\frac{1}{r}\frac{\partial \chi}{\partial z}, \quad w = \frac{1}{r}\frac{\partial \chi}{\partial r} \tag{72}$$

Using Eq. (5) we find

$$\frac{\chi}{R^2 U/2} = 2f(\eta)\xi + \alpha \int_1^{\eta} g(\eta)\mathrm{d}\eta \tag{73}$$

Here $\alpha = W/U$ is the ratio of axial velocity to injection velocity. Figs. 7 and 8 show some representative streamlines. It is seen that any axial motion of the cylinder skews the streamline pattern.

The longitudinal shear stress on the inner cylinder τ_l is given as

$$\frac{\tau_l}{2\mu U/R} = 2f''(1)\xi + \alpha g'(1) \tag{74}$$

where $\mu = \rho\nu$ is the dynamic viscosity of the fluid. The azimuthal shear stress τ_a is found to be

$$\frac{\tau_a}{\mu\Omega} = 2h'(1) - 1 \tag{75}$$

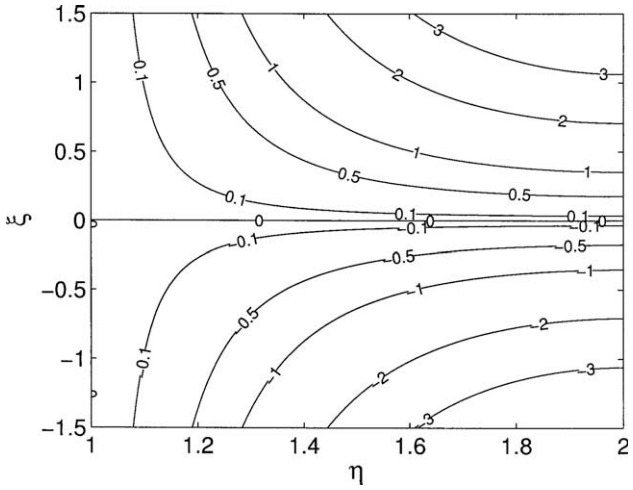

Fig. 7. The normalized stream function $\frac{\chi}{R^2U/2}$ with $b = 2$, $Re = 1$,$\alpha = 0$. Fluid is injected from the outer cylinder at $\eta = 2$ towards the inner cylinder at $\eta = 1$. The dashed line stands for the stagnation streamline.

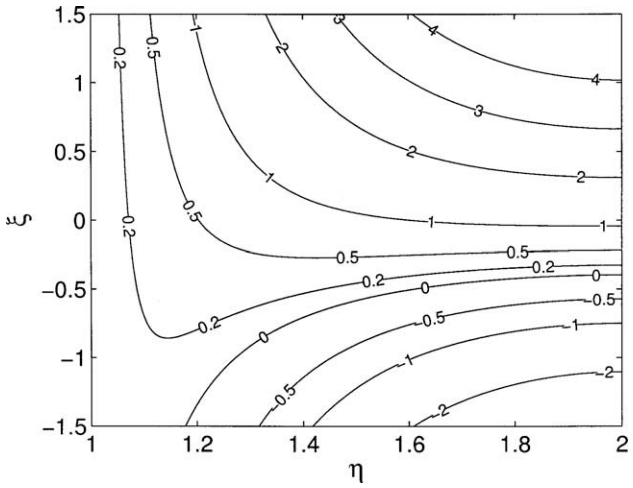

Fig. 8. The normalized stream function $\frac{\chi}{R^2U/2}$ with $b = 2$, $Re = 1$, $\alpha = 3$.

Let D be the longitudinal drag and L be the length of the annulus. Integrating Eq. (74) over the inner surface gives

$$\frac{D}{\pi L\mu W} = 4g'(1) \tag{76}$$

Let M be the moment or toque experienced by the rotation. Then

$$\frac{M}{\pi LR^2\mu\Omega} = 4h'(1) - 2 \tag{77}$$

We see that all these properties are related to the boundary derivatives in Table 1.

7. Heat transfer problem

The axisymmetric energy conservation equation is [13]

$$c_p(uT_r + wT_z) = \frac{\lambda}{\rho}\left(T_{rr} + \frac{T_r}{r} + T_{zz}\right) + \nu\left[2\left(u_r^2 + \frac{u^2}{r^2} + w_z^2\right) + \left(v_r - \frac{v}{r}\right)^2 + v_z^2 + (u_z + w_r)^2\right] \tag{78}$$

where λ is the thermal diffusivity and T is the temperature. Assume the temperature of the outer cylinder is held constant at T_b and that of the inner cylinder at T_1. Let

$$T = T_b + (T_1 - T_b)[k(\eta)\xi^2 + q(\eta)\xi + s(\eta)] \tag{79}$$

Three similarity equations are derived from Eq. (78).

$$\eta k'' + k' + Re\,Pr\cdot(fk' - 2f'k) + 4PrEc\cdot\eta f''^2 = 0 \tag{80}$$

$$\eta q'' + q' + Re\,Pr\cdot(fq' - f'q - \alpha g k) + 4\alpha PrEc\cdot\eta f''g' = 0 \tag{81}$$

$$2\eta s'' + 2s' + k + Re\,Pr\cdot(2fs' - \alpha g q) + PrEc\cdot\left[\left(\frac{2f^2}{\eta^2} + 8f'^2 - \frac{4ff'}{\eta}\right)\cdot + 2\alpha^2\eta g'^2 + \beta^2\left(2\eta h'^2 - 2hh' + \frac{h^2}{2\eta}\right)\right] = 0 \tag{82}$$

where $\mathrm{Pr} = \nu\rho C_p/\lambda$ is the Prandtl number; $Ec = U^2/[C_p(T_1 - T_b)]$ is the Eckert number; $\alpha = W/U$, $\beta = \Omega a/U$ are velocity ratios. The boundary conditions are

$$k(1) = 0, \quad k(b) = 0, \quad q(1) = 0, \quad q(b) = 0, \quad s(1) = 1, \quad s(b) = 0 \tag{83}$$

Although Eqs. (80)–(83) can be integrated as before, we shall only illustrate with the non dissipative case. For small velocities, Let $U^2 \ll C_p(T_1 - T_b)$, the equations show

$$k = 0 \tag{84}$$

$$q = 0 \tag{85}$$

$$\eta s'' + s' + Re\,Pr\cdot fs' = 0 \tag{86}$$

The solution of Eq. (86) is

$$s = \int_\eta^b \frac{1}{x}\exp\left(Re\,Pr\cdot\int_x^b \frac{f(t)}{t}\mathrm{d}t\right)\mathrm{d}x \Big/ \int_1^b \frac{1}{x}\exp\left(Re\,Pr\cdot\int_x^b \frac{f(t)}{t}\mathrm{d}t\right)\mathrm{d}x \tag{87}$$

Define a Nusselt number $Nu = 2Rq/\lambda(T_1 - T_b)$ where q is the heat transfer per area. Then

$$Nu = -4s'(1) \tag{88}$$

The Prandtl number is about 0.7 for gasses, 7 for water, and much higher for oils. Table 2 shows our results. We note that Eqs. (80)–(82) can be similarly integrated even when dissipation is included.

8. Discussions

We have found a rare similarity solution of the 3D Navier–Stokes equations in an annular region. Our numerical results are particularly important for pressure- lubricated bearings. Our approximate asymptotic solutions are also useful in their various regions of validity. Note that convergence is not a necessity for asymptotic expansions [14].

We assumed constant density and constant viscosity. Effects such as compressibility, dependence of viscosity on temperature, shear and pressure have not been addressed. The effect of temperature on viscosity is well known, while the effects of shear and pressure have been delineated by definitive works of Malek and Rajagopal [15–17]. However, for miniature gas injection bearings modeled in this paper these effects may be minimal. The density variation is small due to the low Mach number. The pressure needed is small, being proportional to length (volume over area). The temperature is controlled since

Table 2a
Nusselt number with $b = 1.1$ in Eq. (87)

*Pr**Re*	0.1	1	10	100	1000	10,000
0.7	42.40	42.40	42.41	42.48	42.57	42.61
7	46.26	46.28	46.38	47.06	48.05	49.04
70	78.88	78.96	79.89	86.27	97.04	102.95
700	181.82	182.16	185.41	208.77	261.34	306.69

Table 2b
Nusselt number with $b = 2$ in Eq. (87)

*Pr**Re*	0.1	1	10	100	1000	10,000
0.7	6.27	6.28	6.36	6.47	6.53	6.55
7	10.08	10.18	10.86	12.06	12.75	13.01
70	22.36	22.72	25.25	31.16	36.38	39.05
700	48.52	49.40	55.86	73.07	95.10	112.80

fluid is being continuously replenished and for simple gases shear dependence is almost nil. If any of these effects becomes important, similarity is destroyed and full numerical integration of the partial differential equations will be necessary.

It is found that when the cross-flow Reynolds number is low, the annular region is dominated by viscous terms, represented by Eq. (17). On the other hand, if the Reynolds number is high, the domain is dominated by the injection potential flow (Eq. (34)), and a boundary layer exists near the moving inner cylinder. The zeroth order approximation for small gap width, where the flow is mostly parallel, is related to the much- used lubrication theory. Our formulas also give error estimates in the different asymptotic expansions.

Both drag and moment experienced by the inner cylinder are increased by increased Reynolds number and/or decreased gap width. The heat transfer is increased by the Reynolds number only minimally, but is increased more by higher Prandtl numbers and smaller gap widths.

The streamlines (Fig. 8) show the interaction of longitudinal motion with the cross-flow injection. A detailed flow field is useful for mass transfer and mass deposition problems.

It is hoped that our paper would elicit more numerical and experimental work in this interesting area.

Appendix

Solutions to Eqs. (26)–(28).

$$
\begin{aligned}
f_1 = {} & C_2 + C_3\eta + C_4\eta^2 + [288(-1+b)^2 b\eta^2 + 72C_1(-1+b)^4\eta - 108(-1+b)b\ln b\cdot\eta^2 \\
& + 5(-1+b)b\ln b\cdot\eta^3 - 72C_1(-1+b)^3(1+b)\ln b\cdot\eta - 6b\ln^2 b\cdot\eta^3 + b\ln^2 b\cdot\eta^4 \\
& + 18C_1(-1+b^2)^2\ln^2 b\cdot\eta - 72(-1+b)^2\eta(3b\eta + C_1 - 2bC_1 + b^2C_1)\ln\eta \\
& - 6(-1+b)\ln b\cdot\eta(-12b\eta + b\eta^2 - 12C_1 + 12bC_1 + 12b^2C_1 - 12b^3C_1)\ln\eta \\
& - 18C_1(-1+b^2)^2\ln^2 b\cdot\eta\ln\eta + 36(-1+b)^2 b(-\eta+\eta^2)\ln^2\eta \\
& + 18(-1+b)b\ln b\cdot\eta\ln^2\eta]/[18(-1+b)^2(2-2b+(1+b)\ \ln b)^2] \\
g_1 = {} & -\sqrt{b}\{2\ln^3\eta(3-4\eta+\eta^2-\ln\eta) - 72(-1+b)^2\ln\eta \\
& + \ln^2\eta\{(-1+\eta)(-37+16b+3\eta) - 2[5-8\eta+\eta^2+b(-2+4\eta)]\ln\eta + 2 + \ln^2\eta\} \\
& + (-1+b)\ln\eta[72(-1+\eta) + (37+21b-40\eta)\ln\eta \\
& + (-4+8\eta)\ln^2\eta]\}/\{4(-1+b)\ln^2\eta[2-2b+(1+b)\ln\eta]\} \\
h_1 = {} & \sqrt{b}\Big\{\cosh\left(\frac{\ln\eta}{2}\right)\{\ \ln b\{-(-1+\eta)[-3b^2(-2-5\eta+\eta^2) + \eta(11-7\eta+2\eta^2)] + 6(\eta+3b^2\eta)\ln\eta\} \\
& - 3(-1+b)\{(-1+\eta)[3(-3+\eta)\eta - 4b^2(1+2\eta)] + 2\eta[2+2\eta-\eta^2+2b^2(2+\eta)]\ln\eta \\
& + 2b^2\eta\ln^2\eta\}\} + \Big\{-\eta\coth\left(\frac{\ln\eta}{2}\right)[3(-1+b)^2(9+b+8b^2) + 6(1+2b^2+b^3)\ln^2 b \\
& + (23-12b+24b^2-26b^3-9b^4)\ln b] + \ln b[10b^3\eta - 9b^4\eta + b^2(6+9\eta+6\eta^2-3\eta^3) \\
& + \eta(-12-6\eta-3\eta^2+2\eta^3) + 6(1+b^2)\eta\ln\eta] + 3(-1+b)\{8b^3\eta + \eta^2(4+3\eta) \\
& - b^2(4+3\eta+8\eta^2) - 2\eta[2-2(-1+b^2)\eta+\eta^2]\ln\eta + 2b^2\eta\ln^2\eta\} \\
& - 6(1+b^3)\eta\ln^2\eta\Big\}\sinh\left(\frac{\ln\eta}{2}\right)\Big\}\Big/\{6(-1+b)^2(1+b)\eta[2-2b+(1+b)\ln b]\}
\end{aligned}
$$

References

[1] C.Y. Wang, Exact solutions of the steady-state Navier–Stokes equations, Ann. Rev. Fluid Mech. 23 (1991) 159–177.
[2] K. Hiemenz, Die Grenzschicht an einem in den gleichformingen Flussigkeitsstrom eingetauchten graden Kreiszylinder, Dinglers Polytech. J. 326 (1911) 321–324.
[3] C.Y. Wang, Axisymmetric stagnation flow on a cylinder, Quart. Appl. Math. 32 (1974) 207–213.
[4] R.S.R. Gorla, Nonsimilar axisymmetric stagnation flow on a moving cylinder, Int. J. Eng. Sci. 16 (1978) 397–400.
[5] G.M. Cunning, A.M.J. Davis, P.D. Weidman, Radial stagnation flow on a rotating circular cylinder with uniform transpiration, J. Eng. Math. 33 (1998) 113–128.
[6] S.R. Choudhury, Y. Jaluria, Forced convection heat transfer from a continuously moving heated cylindrical rod in materials processing, J. Heat Trans. 116 (1994) 724–734.
[7] S. Heller, W. Shapiro, O. Decker, A porous hydrostatic gas bearing for use in miniature turbomachinery, ASLE Trans. 14 (1971) 144–155.
[8] B.C. Majumdar, Analysis of externally pressurized porous gas bearings-1, Wear 33 (1975) 25–35.
[9] V.P. Castelli, Experiment and theoretical analysis of the gas-lubricated porous rotating journal bearing, ASLE Trans. 22 (1979) 382–388.
[10] J.C.T. Su, H.I. You, J.X. Lai, Numerical analysis on externally pressurized high-speed bearings, Ind. Lub. Trib. 55 (2003) 244–250.
[11] I.F. Santos, R. Nicoletti, A. Scalabrin, Feasibility of applying active lubrication to reduce vibration in industrial compressors, J. Eng. Gas Turbine Power 126 (2004) 848–854.
[12] H. Schlichting, Boundary Layer Theory, 7th ed., McGraw-Hill, New York, 1979.
[13] S.W. Yuan, Foundations of Fluid Mechanics, Prentice-Hall, New Jersey, 1971.
[14] M. Van Dyke, Perturbation Methods in Fluid Mechanics, Parabolic, Stanford, 1975.

[15] J. Hron, J. Malek, K.R. Rajagopal, Simple flows of fluids with pressure-dependent viscosities, Proc. Roy. Soc. Lond. A457 (2001) 1603–1622.
[16] J. Malek, J. Necas, K.R. Rajagopal, Global existence of solutions for flows of fluids with pressure and shear dependent viscosities, Appl. Math. Lett. 15 (2002) 961–967.
[17] M. Franta, J. Malek, K.R. Rajagopal, On steady flows of fluids with pressure and shear dependent viscosities, Proc. Roy. Soc. Lond. A461 (2005) 651–670.